Workshop on Visualisation in Environmental Sciences (EnvirVis) (2026)
K. Feige, B. Nsonga, and K. Rink (Editors)

Visualization of Temporal Changes in Environmental Point Cloud Scans

Gorazd Gorup and Ciril Bohak

University of Ljubljana, Faculty for Computer and Information Science, Slovenia

Figure 1: *A render of a UAV point cloud with M3C2 distances overlaid in regions of significant change.*

Abstract

Expert analysis of environmental point clouds is often overwhelmed by the volume of raw data. This study introduces an integrated visualization approach to simplify the detection of temporal surface changes. By developing a prototype that identifies and displays rockfall and deposition areas, we bridge the gap between complex geomorphological data and intuitive visual feedback. In addition to expert tools, we present a method for generating animated cliff displays to communicate environmental risks to the general public. We evaluate the effectiveness of these visualizations and discuss the trade-offs of using the M3C2 algorithm for volumetric analysis, concluding that visual synthesis is an essential tool for modern geomorphological research.

CCS Concepts Categories and Subject Descriptors** (according to ACM CCS): **I.3.3 [Computer Graphics]: Human-centered computing —Geographic visualization

1. Introduction

Observation of coastal cliffs is essential in areas accessible to the general public, as natural processes such as denudation or spontaneous rockfalls can endanger people walking at the base of the cliffs. Experts analyze morphological changes over time to predict potential rockfalls and prevent the public from accessing critical areas. Technologies such as Light Detection and Ranging (LiDAR) and photogrammetry, which capture land surfaces in great detail, are used to scan the surface at different times. The resulting scans, in the form of point clouds, are then compared to observe changes in material volume within the cliff composition.

It is difficult to determine changes from raw point cloud overlays because points represent only small, discrete samples of a surface, and gaps between samples hinder visual comparison. Noise in the captured data and the need to compare multiple pairs of scans over time further exacerbate this problem.

Existing workflows for point-cloud-based terrain monitoring in software such as CloudCompare[†] or MeshLab [CCC*08] typically require manual preprocessing, conversion of point clouds to other

† https://www.cloudcompare.org/

DOI: 10.2312/envir.20261004

representations, and calculation of differences or volumes with varying quality. There is also a need to inform the general public about the nature of processes on cliffs and their potential dangers.

In this paper, we present three methods to visualize coastal cliffs captured with Terrestrial Laser Scanning (TLS) and Unmanned Aerial Vehicle (UAV), highlighting morphological changes. Specifically, we designed:

- a visualization technique for observing cumulative changes in point clouds over different time spans,
- a method for identifying and visualizing areas with significant change and their associated volume differences,
- and a simulation-based visualization of material breaking away.

The first two visualizations are intended to help experts analyze changes by highlighting regions on the surface with informative overlays. In addition to expert analysis, we identified a need to communicate cliff dynamics and associated risks to the public in an accessible way, which we addressed with the third visualization. This visualization is illustrative and not necessarily accurate; it is not intended for expert analysis. We implemented the visualizations as a prototype extension for the 3D modeling software Blender[‡]. We tested our work on a real use case involving scanned cliffs along the Slovenian coast, where rockfalls threaten people and assets along the coastal pathways. We further refined the workflow based on feedback from domain experts involved in cliff monitoring.

The paper is organized as follows: Section 2 discusses related work, Section 4 describes our methods and contributions, Section 5 presents our experimental data and findings, and Section 6 provides the conclusion and outlines future work based on the results.

2. Related Work

Multiple studies have analyzed land for risk management and monitoring. Abellán *et al.* [AVC*11] studied Spanish cliffs to identify potential rockfalls by capturing TLS data over two years. They aligned the point clouds using the Iterative Closest Point (ICP) algorithm [RL01] and computed differences between consecutive point clouds with PolyWorks® software[§]. Eker *et al.* [EAH17] similarly observed changes in a forested region in Austria before and after a landslide, using a combination of UAV-produced and LiDAR point clouds. For volume difference computation, they used the Multiscale Model to Model Cloud Comparison (M3C2) algorithm to determine the overall shift in ground material. Terefenko *et al.* [TPG*19] used several years of TLS surveys to detect morphological changes in coastal cliffs. They built Digital Elevation Models (DEMs) from point clouds and extracted features such as contours, rapid height change, and volume change, then used Bayesian networks to model erosion. TLS data was also used in [HCH11] to visualize changes in the Californian coastline. The system featured an interactive virtual environment with paintbrush tools and overlays of changes.

Chen [Che19] proposes visualization techniques that integrate environmental sensor data with graphical representations, such as markers with informative pop-ups, to enable intuitive exploration of spatial and temporal trends in environmental quality. Similar marker-based visualizations are also used in [BMB*17] to highlight soil types in 3D environmental data.

A substantial body of research has addressed change detection in multi-temporal point clouds, particularly for quantifying geomorphological change and estimating volumetric differences between scans. A widely used approach is presented in [LBL13], which introduced the M3C2 algorithm. This method measures distances directly between two point clouds along local surface normals, avoiding intermediate meshing or DEM generation and enabling statistically robust detection of surface change in complex terrain. Several studies have applied M3C2 or similar point-based comparisons to detect and quantify geomorphic change in photogrammetric and LiDAR datasets. For example, [DHE*20] used dense image-matching point clouds from multi-temporal image sequences and computed M3C2 distances to identify surface displacement and deformation over time, demonstrating the suitability of photogrammetric point clouds for monitoring slope movement. A similar distance computation approach was used in [TA14], along with clustering and spatial pattern recognition, to detect rockfalls. [AGGG20] employed M3C2 for change detection and computed the volume of change by projecting M3C2 values onto optimally rotated planes.

3. Data

We used data collected during the Slovenian research project *Erosional Processes on Coastal Flysch Cliffs and Their Risk Assessment*, which evaluated the suitability of remote scanning data for analyzing Slovenian cliffs [KKT25]. The researchers generated 10 TLS and 8 UAV point clouds of the Strunjan coastal cliffs at various times between April 2019 and April 2024. For this paper, we focused on a smaller region above Moon Bay, as TLS data were limited to that area. We observed that UAV data were collected between November 2020 and March 2024 and do not always coincide with the TLS acquisition times. The analyzed region covers approximately 250 meters of cliff length and up to 80 meters in height.

TLS point clouds were used for visualizations in this paper, while UAV scans were used to project color information onto the TLS points. TLS clouds contain an average of 31 million points, which

Capture date	Points	Subsampled points
April 2019	31,478,338	431,379
January 2020	32,734,266	470,294
November 2020	31,115,720	438,688
April 2021	25,881,779	372,095
October 2021	25,351,286	375,594
March 2022	33,010,916	503,837
October 2022	27,729,922	466,517
April 2023	35,767,567	527,536
January 2024	34,537,167	484,752
April 2024	33,228,633	569,345

Table 1: *List of TLS point clouds, their capture dates, the number of points in the original scan, and the number of points after the subsampling step.*

‡ https://www.blender.org/

§ https://hexagon.com/products/polyworks

Table 2: *List of UAV point clouds, their capture dates, the amount of points in the original scan, and the amount of points after the subsampling step.*

Capture date	Points	Subsampled points
November 2020	158,103,676	1,018,365
March 2021	152,491,956	872,095
March 2022	90,205,478	693,989
December 2022	116,260,346	818,583
April 2023	95,444,041	660,171
September 2023	99,254,699	817,840
March 2024	102,279,504	645,802

include information about normals and intensities but lack color information. The point clouds were provided with vegetation already filtered out. Each UAV scan, stored in LASer (LAS) format, has an average of 116 million points and contains color information and other LiDAR data. The details of the point clouds are listed in tables 1 and 2.

4. Method Overview

Our visualization pipeline consists of three main stages: preprocessing multi-temporal point clouds, extracting significant morphological changes, and visualizing results through interactive overlays and animated simulations. We developed our visualizations as a prototype system using Blender's Python API. The workflow overview is shown in Figure 2.

4.1. Preprocessing

Preprocessing was carried out using a combination of CloudCompare and custom scripts. All point clouds were initially aligned and moved to the center of the global coordinate system to prevent floating-point errors caused by large point coordinates when importing them into Blender. Fine-grained alignment between point clouds was achieved using the ICP algorithm [BM92, CM92, RL01], with the RMS difference set to 1.0×10^{-5}. To reduce processing time, we subsampled the clouds by decreasing the octree depth to 10. We then computed the M3C2 distance [LBL13] between consecutive point clouds, which measures surface change along the local surface normal. The differences are negative (rockfall) or positive (accumulated material). We empirically determined M3C2 parameter values that produced best result on representative cliff sections.

We chose a cylinder radius of 2.0 to ensure a sufficient number of neighboring points for stable distance estimation while still preserving localized cliff changes. Smaller radii produced noisier measurements in sparsely sampled regions, while larger radii oversmoothed narrow material displacements. The normal radii of 0.1 and 1.0 enabled estimation of both fine-scale surface orientation and broader local surface trends, which improved robustness on irregular cliff geometry. The maximum cylinder height of 10.0 was selected to accommodate larger displacements and avoid truncating substantial rockfall regions.

We further converted TLS point clouds into mesh geometry using Delaunay triangulation. This method produces artifacts and large triangles to fill gaps in the data, which in our case did not enhance the visualization. We chose to remove them during the rendering stage rather than at this stage, as the filled geometry could then be used to simulate rockfall.

4.2. Temporal Change Visualization

We projected the differences onto mesh geometry derived from TLS. Because the sign of M3C2 distance values is important, we mapped them to a color gradient to show the nature and intensity of change at each point.

We imported TLS point clouds into Blender and used its Geometry Nodes feature to map distances from a specified range of clouds onto the mesh, as shown in figure 3. The clouds are iterated, and the values at the nearest points for each mesh vertex are summed.

4.3. Significant Change Visualization

We aimed to present areas with locally significant changes. We placed markers above these areas to indicate the significance of the change using color and to show the volume of the removed or added material with text on the markers. To display the surface of cliffs, we used the reconstructed mesh described in section 4.1.

First, we filtered the points to remove unimportant changes and noise. The M3C2 distance of each point was compared to a threshold, and points with lower values were discarded. The remaining points formed highly fragmented clusters, which were still affected by noise and abrupt changes. Therefore, we applied Gaussian smoothing to the points to merge small neighboring clusters that likely belonged to the same local change. Gaussian smoothing reduces noise while preserving the spatial structure of local change regions. We performed this in the following steps:

1. We built a *k-d* tree structure from the points to efficiently search for the nearest neighbors of each point.
2. For each point, we retrieved the neighboring points and their respective M3C2 distances, and computed the smoothed distance using the following formula:

$$v_{\text{smooth}} = \frac{1}{2\pi\sigma^2} \sum_{i=1}^{n} v_i e^{-\frac{d_i^2}{2\sigma^2}}, \tag{1}$$

where σ is the standard deviation parameter, n is the number of neighboring points, d_i is the Euclidean distance from the point to neighbor i, and v_i is the M3C2 distance at neighbor i.

The threshold applied to the M3C2 distances was intended to suppress low-magnitude fluctuations caused by measurement uncertainty, noise, and surface roughness. We selected the threshold empirically by comparing filtered and unfiltered results on representative scans and choosing the smallest value that consistently removed visually insignificant changes while preserving clearly identifiable erosion and deposition regions.

The Gaussian smoothing parameter σ was chosen so that the neighborhood effect at each point was strong enough to suppress outliers, while avoiding excessive blending of values between neighboring areas with unrelated changes (positive or negative).

We then divided the points into two groups based on the sign of the M3C2 distance. At this stage, we used the original values, not

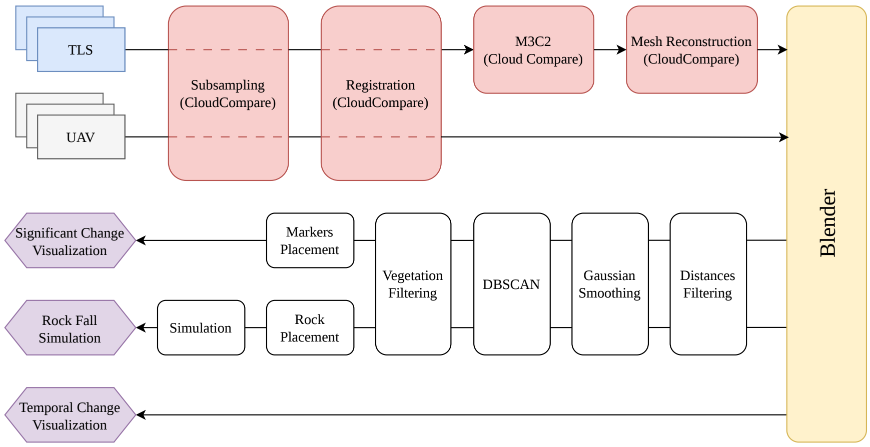

Figure 2: *A diagram showing the visualization process. Our inputs are TLS and UAV data that are transformed in CloudCompare before being imported in Blender. Then Python scripting and Geometry Nodes are used to produce each of the three visualizations.*

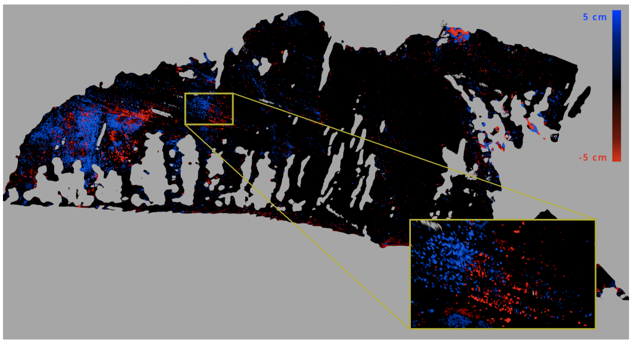

Figure 3: *Visualization of accumulated change from April 2019 to November 2020. Blue indicates added material, while red indicates removed material. The changes are projected onto the mesh from the April 2019 scan.*

the smoothed ones. Points in each group were clustered using the DBSCAN [EKS*96] algorithm with $\epsilon = 1.5$ and a minimum of 10 points. For each cluster, we approximated the volume of change using the following formula:

$$V \approx a \sum_{i=1}^{m} v_i, \tag{2}$$

where a is the approximate average area at each point in the scan, m is the number of points in the cluster, and v_i is the M3C2 distance at point i.

The DBSCAN parameters were selected based on the average point spacing after subsampling and the expected spatial extent of meaningful geomorphological events. The chosen ϵ value enabled neighboring points within the same local area of change to form coherent clusters while preventing excessive merging of nearby but distinct changes. The minimum cluster size filtered out isolated noisy detections while preserving visually relevant cliff changes. We observed that the resulting clusters remained stable under moderate variations of these parameters; however, substantially increasing ϵ led to overmerged regions, while decreasing it produced fragmented clusters.

We also used the uncertainty produced by the M3C2 algorithm for each point and calculated the overall uncertainty as:

$$U \approx \sum_{i=1}^{m} u_i, \tag{3}$$

where m is the number of points in the cluster, and u_i is the M3C2 uncertainty at point i.

Some changes are caused by vegetation and do not reflect morphological changes in the cliffs themselves. We filtered out clusters identified as associated with vegetation points. Vegetation was removed from the TLS scans according to [KKT25], using geometric feature filtering. We searched for gaps in the reconstructed mesh and marked those points or vertices as vegetation. If a cluster contained more than a certain number of vegetation points, we removed it.

We then generated markers above each cluster. We computed the center of each region on the XY plane, c_{xy}, to position the markers in the middle of the cluster. The marker height was set to the maximum elevation within the cluster to avoid intersection with the surface. We colored and resized the markers based on the M3C2 values. First, the uncertainty was compared to a chosen threshold. In our case, we set the threshold to $\frac{v_i}{2}$, where v_i is the M3C2 distance. This heuristic threshold was chosen empirically to distinguish visually stable regions from regions dominated by uncertainty-related artifacts in the evaluated datasets. If the uncertainty was too great, the marker was colored gray; otherwise, it was colored based on the sign of the M3C2 distance: red for negative distances and blue for positive distances. The size of the markers was determined by

$$s = \ln \left| \sum_{i=1}^{m} v_i \right|, \tag{4}$$

where m is the number of points in the cluster, and v_i is the M3C2 distance at point i. Above the markers, text showing distances and uncertainties was placed. Figure 4 shows the final visualization.

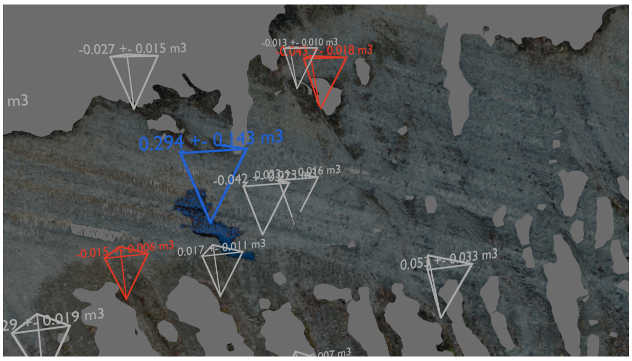

Figure 4: *Markers indicate areas of potentially significant change on the cliff surface. Red areas show removed material, while blue areas show accumulated material. Grey markers represent changes with high uncertainty. The blue marker at the center of the image is selected, and its cluster is shown colored on the mesh. Based on its value and size, this appears to be the most significant change in the visualized area.*

The uncertainty values are intended to support risk-aware interpretation of detected changes rather than serve as strict confidence intervals. Regions with low uncertainty can be interpreted as reliable indicators of localized geomorphological change, while high-uncertainty regions may reflect residual vegetation artifacts or noise. Gray markers act as visual indicators that the corresponding change regions should be interpreted cautiously and may require additional manual inspection or comparison with the original point clouds before use in geological assessment or hazard-related decision-making.

We enabled interaction with the markers. Each marker could be selected. Upon selection, the cluster pertaining to that marker would be colored to show the extent of change. The colors used were derived from the original M3C2 distances, not smoothed ones.

4.4. Rockfall Simulation

As the final visualization, we created animated representations of rockfalls using real-world data. This visualization serves as a valuable tool for raising public awareness about morphological changes on the Strunjan cliffs and the potential risks associated with rockfalls. It is intended as a qualitative illustration rather than a physically accurate rockfall model.

The visualization was developed from the results presented in section 4.3. After identifying clusters of significant change, we generated simplified 3D rock models at each cluster with negative change (indicating material removal), instead of using markers. The objects were scaled as described in equation 4. We simulated the rockfall using Blender Rigid Body physics. The reconstructed mesh from the point cloud was used for collision detection. Delaunay triangulation was applied to fill gaps in the data, which helped prevent the objects from falling through the surface. Rock objects were treated as dynamic rigid bodies, while the surface mesh was treated as a static rigid body. The visualization is shown in figure 5.

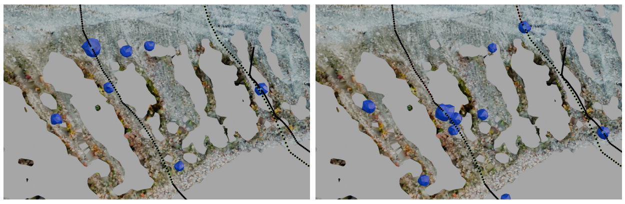

Figure 5: *Two frames of the animation. The rocks are colored blue to make them easily distinguishable from the background and the cliff surface. For three of the rock objects, motion paths have been precomputed (green lines with black dots).*

4.5. Rendering Details

When reconstructing a mesh from a point cloud, as described in Section 4.1, gaps in the data are also filled, resulting in large triangles that disrupt the continuity of the mesh. Therefore, we chose to hide these before rendering. Using Geometry Nodes, we identified triangles exceeding an area threshold and removed them.

For surface rendering, a simple material was used that combined the color of the underlying points with the M3C2 distances. The distances were normalized to the interval [0, 1] and mapped to colors ranging from red to blue using a color ramp. Since TLS data was used in most renders and the original point clouds do not contain color, this information had to be obtained from UAV point clouds. Geometry Nodes were applied to the mesh surface; for each vertex, the nearest point in the UAV point cloud was found, and its color information was assigned to the vertex.

5. Evaluation

Our evaluation focuses on assessing whether the proposed visualization prototype supports the interpretation of multi-temporal coastal cliff changes by enabling:

- identification of significant erosion and deposition regions,
- contextual interpretation of detected changes, and
- communication of geomorphological processes to both domain experts and non-expert audiences.

The evaluation combines quantitative analysis of detected change regions with qualitative feedback collected from domain experts during interactive exploration sessions. Due to the limited availability of expert participants and the exploratory nature of the prototype, the evaluation is intended as an initial assessment rather than a controlled user study.

We evaluated our prototype using multi-temporal scans of the Strunjan coastal cliffs. We present results from scans taken in April 2019 and January 2020, as this interval includes several localized erosion events while maintaining manageable visual complexity. Based on [KKT25], the average area of a point was determined to be $0.00256\,\mathrm{m}^2$.

5.1. Assessment of Visualization Methods

The prototype was evaluated using three distinct visualization techniques designed to meet the needs of both experts and the general public.

We conducted informal evaluation sessions with four researchers familiar with coastal geomorphology and point-cloud-based terrain analysis. Participants interacted with the prototype using the Strunjan dataset to inspect erosion regions. They also received a detailed list of detected regions, including images of affected areas, their uncertainties, and M3C2 distances for separate inspection. Feedback was collected through semi-structured discussions focused on interpretability, usability, and perceived analytical value.

5.1.1. Temporal and Cumulative Change Analysis

The cumulative change visualization highlighted surface evolution by projecting M3C2 distances onto the mesh geometry. Normalizing these distances to a $[0, 1]$ interval and mapping them to a red-to-blue color ramp provided a clearer visual overview of the cliff face, providing an immediate overview of erosion and deposition patterns.

To enhance interpretability, we used a "hybrid" approach by projecting color information from UAV scans onto the high-resolution TLS geometry. Experts reported that the integrated color context helped distinguish actual morphological changes from residual noise, as the natural color context provided important cues for identifying vegetation-related artifacts.

5.1.2. Quantitative Analysis Results

Our system detected 24 regions of significant change, primarily on the steeper, erosion-prone left side of the cliff. The quantitative precision of the prototype is demonstrated by the following findings:

- **Volume Totals:** We identified 10 regions of negative change totaling $0.525\,\mathrm{m}^3$ of removed material and 14 regions of positive change totaling $0.340\,\mathrm{m}^3$ of added material.
- **Cluster Density:** Each region contained an average of 287 points, indicating that the DBSCAN parameters ($\epsilon = 1.5$, minimum 10 points) produced clusters that corresponded to visually identifiable geomorphological events.
- **Filtering Success:** A threshold of 10 vegetation points effectively removed most vegetation-induced markers while retaining critical geological data.

A key feature for expert trust was the handling of uncertainty. The average uncertainty per region (0.018) was higher than the average volume (0.007), supporting the use of gray markers for high-uncertainty or insignificant changes. Experts reported that uncertainty-aware markers were useful for distinguishing between regions likely representing genuine geomorphological changes and regions potentially influenced by vegetation remnants or sparse sampling. In practice, high-uncertainty markers were interpreted as indicators requiring additional verification rather than definitive evidence of erosion or deposition.

5.1.3. Parameter Choices

In significant change visualization (Section 4.3), certain parameters had to be set for our specific use case. The M3C2 cylinder radius, normal neighborhood radii, and DBSCAN's ϵ all depend heavily on point cloud density. For more general processing, this relationship would need to be studied to determine whether appropriate values can be computed from the point cloud structure. If the M3C2 cylinder radius is too small, significant changes in the neighborhood may be missed because relevant points are not included in the compared point clouds. Conversely, if the radius is too large, it may include points at similar heights as the observed point, causing the average distance to become too small. If DBSCAN's ϵ is too high, it may cluster too many points together; if it is too low, it may create too many granular regions.

M3C2's maximum cylinder height determines how large of a displacement we still detect. This parameter depends on spatial size of the point cloud and the expected volume displacement.

5.1.4. Rockfall Simulation for Public Engagement

For qualitative illustration, we generated animated rockfalls at clusters where material removal was detected. To ensure these objects were easily distinguishable from the complex cliff background, we used blue rock models. This color choice, combined with motion paths, serves as an effective tool for raising public awareness about the spontaneous nature of cliff denudation and associated safety risks.

5.2. Methodological Constraints

The current evaluation has several limitations. The expert assessment was exploratory and involved a limited number of participants rather than a controlled user study. As a result, the findings primarily demonstrate the feasibility and perceived interpretability of the approach, rather than statistically generalizable improvements in analytical performance. Future work should include task-based evaluations with larger participant groups and comparisons with existing geomorphological analysis workflows.

The uncertainty in the estimated volumes is likely due to residual vegetation and the necessary use of subsampled point clouds. Additionally, although Delaunay triangulation was used to fill data gaps for the simulation, it sometimes produced artifacts. However, experts found visualizing these "gaps" useful for understanding exactly where data was missing because of the original vegetation filtering.

6. Conclusion and Future Work

In this work, we present three visualization techniques for analyzing geomorphological changes over time in point clouds of coastal cliffs. The proposed methods include cumulative change visualization, a marker-based representation of significant local changes with estimated volume differences, and an animation-based visualization illustrating potential rockfall events. We implemented these techniques in a prototype system and evaluated them using multi-temporal scans of the Strunjan coastal cliffs.

The case study shows that the visualizations effectively highlight regions of erosion and deposition and provide intuitive representations of local cliff dynamics. The marker-based visualization enables users to quickly identify areas of significant change, while the cumulative change visualization offers an overview of surface evolution over longer time spans.

The current approach has several limitations. Volume estimation based on M3C2 distances provides only an approximate measure of material change and may overestimate volumes in certain geometries. Additionally, residual vegetation and the use of subsampled point clouds introduce uncertainty in the detected change regions. Manual adjustment of parameters for generating clusters is required for each dataset, which demands in-depth knowledge of the underlying algorithms. The prototype could also benefit from improved readability and better occlusion handling of annotations.

Future work will focus on improving the robustness of volume estimation, refining clustering and filtering techniques for detecting significant changes, and automating parameter selection to reduce manual tuning. To address challenges related to data gaps and artifacts in reconstructed meshes, we plan to explore advanced hole-filling and surface-completion techniques. Specifically, we will investigate the use of LiDAR data augmentation methods, such as those proposed by Bohak *et al.* [BSKM20], to generate synthetic points that preserve the structural integrity of the cliff surface while minimizing visual noise. Additional enhancements to the visualization interface and rockfall simulation, including more realistic physics and improved occlusion handling for annotations, could further enhance the communication of complex cliff dynamics to both domain experts and the general public.

Acknowledgements

The research was conducted within the project Geospatial Information Technologies for Resilient and Sustainable Society (GeoAI) (GC-0006), funded by the Slovenian Research and Innovation Agency (ARIS).

We also thank the authors of [KKT25], the Faculty of Civil and Geodetic Engineering at the University of Ljubljana, and the Institute of Anthropological and Spatial Studies ZRC SAZU for sharing with us the Slovenian cliff dataset.

References

[AGGG20] Álvaro Gómez-Gutiérrez, Gonçalves G. R.: Surveying Coastal Cliffs Using Two UAV Platforms (Multirotor and Fixed-wing) and Three Different Approaches for the Estimation of Volumetric Changes. *International Journal of Remote Sensing 41*, 21 (2020), 8143–8175. doi:10.1080/01431161.2020.1752950. 2

[AVC*11] Abellán A., Vilaplana J. M., Calvet J., García-Sellés D., Asensio E.: Rockfall Monitoring by Terrestrial Laser Scanning – Case Study of the Basaltic Rock Face at Castellfollit de la Roca (Catalonia, Spain). *Natural Hazards and Earth System Sciences 11*, 3 (2011), 829–841. doi:10.5194/nhess-11-829-2011. 2

[BM92] Besl P., McKay N. D.: A Method for Registration of 3-D Shapes. *IEEE Transactions on Pattern Analysis and Machine Intelligence 14*, 2 (1992), 239–256. doi:10.1109/34.121791. 3

[BMB*17] Balla D., Mester T., Botos A., Novak T. J., Raso J., Zichar M., Karika A.: Possibilities of Spatial Data Visualization with Web Technologies for Cognitive Interpretation. In *2017 8th IEEE International Conference on Cognitive Infocommunications (CogInfoCom)* (Sept. 2017), Ieee, p. 000017–000020. doi:10.1109/coginfocom.2017.8268209. 2

[BSKM20] Bohak C., Slemenik M., Kordež J., Marolt M.: Aerial lidar data augmentation for direct point-cloud visualisation. *Sensors 20*, 7 (2020), 1–17. 7

[CCC*08] Cignoni P., Callieri M., Corsini M., Dellepiane M., Ganovelli F., Ranzuglia G.: MeshLab: an Open-Source Mesh Processing Tool. In *Eurographics Italian Chapter Conference* (2008), Scarano V., Chiara R. D., Erra U., (Eds.), The Eurographics Association. doi:10.2312/LocalChapterEvents/ItalChap/ItalianChapConf2008/129-136. 1

[Che19] Chen P.: Visualization of Real-Time Monitoring Datagraphic of Urban Environmental Quality. *EURASIP Journal on Image and Video Processing 2019*, 1 (Feb. 2019). doi:10.1186/s13640-019-0443-6. 2

[CM92] Chen Y., Medioni G.: Object Modelling by Registration of Multiple Range Images. *Image and Vision Computing 10*, 3 (1992), 145–155. Range Image Understanding. doi:https://doi.org/10.1016/0262-8856(92)90066-C. 3

[DHE*20] Dinkel A., Hoegner L., Emmert A., Raffl L., Stilla U.: Change Detection In Photogrammetric Point Clouds For Monitoring Of Alpine, Gravitational Mass Movements. *ISPRS Annals of the Photogrammetry, Remote Sensing and Spatial Information Sciences V-2-2020* (08 2020), 687–693. doi:10.5194/isprs-annals-V-2-2020-687-2020. 2

[EAH17] Eker R., Aydin A., Hübl J.: Unmanned Aerial Vehicle (UAV)-based Monitoring of a Landslide: Gallenzerkogel Landslide (Ybbs-Lower Austria) Case Study. *Environmental Monitoring and Assessment 190*, 1 (Dec. 2017). doi:10.1007/s10661-017-6402-8. 2

[EKS*96] Ester M., Kriegel H.-P., Sander J., Xu X., et al.: A Density-based Algorithm for Discovering Clusters in Large Spatial Databases with Noise. In *kdd* (1996), vol. 96, pp. 226–231. 4

[HCH11] Hsieh T.-J., Chang Y.-L., Huang B.: Visual Analytics of Terrestrial LiDAR Data for Cliff Erosion Assessment on Large Displays. In *Satellite Data Compression, Communications, and Processing VII* (Sept. 2011), vol. 8157, Spie, p. 81570d. doi:10.1117/12.895437. 2

[KKT25] Kregar K., Kozmus Trajkovski K.: Combining UAV Photogrammetry and TLS for Change Detection on Slovenian Coastal Cliffs. *Drones 9*, 4 (2025). doi:10.3390/drones9040228. 2, 4, 5, 7

[LBL13] Lague D., Brodu N., Leroux J.: Accurate 3D Comparison of Complex Topography with Terrestrial Laser Scanner: Application to the Rangitikei Canyon (N-Z). *ISPRS Journal of Photogrammetry and Remote Sensing 82* (2013), 10–26. doi:https://doi.org/10.1016/j.isprsjprs.2013.04.009. 2, 3

[RL01] Rusinkiewicz S., Levoy M.: Efficient Variants of the ICP Algorithm. In *Proceedings Third International Conference on 3-D Digital Imaging and Modeling* (2001), pp. 145–152. doi:10.1109/im.2001.924423. 2, 3

[TA14] Tonini M., Abellan A.: Rockfall Detection from Terrestrial LiDAR Point Clouds: A Clustering Approach Using R. *Journal of Spatial Information Science*, 8 (June 2014). doi:10.5311/josis.2014.8.123. 2

[TPG*19] Terefenko P., Paprotny D., Giza A., Morales-Nápoles O., Kubicki A., Walczakiewicz S.: Monitoring Cliff Erosion with LiDAR Surveys and Bayesian Network-based Data Analysis. *Remote Sensing 11*, 7 (2019). doi:10.3390/rs11070843. 2